2) With the wattmeter connected to the calorimeter via a matching unit with $s = 0.99$.

The readings of the two instruments for powers in the range 8–10 watts are given in Table I.

TABLE I

COMPARISON OF TORQUE-VANE WATTMETER AND WATER CALORIMETER

	Torque-Vane Wattmeter	Water Calorimeter	Per Cent Difference
1) $s=0.92$			
	9.02 watts	8.89 watts	+1.46
	8.94	8.84	+1.13
	9.65	9.48	+1.80
	9.17	8.85	+3.60
	9.10	8.84	+2.94
	9.19	9 06	+1.44
Average difference between the two instruments 2.1 per cent.			
2) $s=0.99$			
	9.10 watts	8.97 watts	+1.4
	9.02	8.92	+1.1
	8.98	8.85	+1.5
	9.34	9.33	+0.1
	8.94	8.87	+0.8
	9.02	8.82	+2.3
Average difference between the two instruments 1.2 per cent.			

These results have been corrected to allow for the measured attenuation in the connecting waveguide. Furthermore, in case 1) above, the wattmeter readings have been corrected for mismatch using (3), and in case 2) above the small loss of power in the matching transformer has been taken into account.

Since the attenuation through the double-vane wattmeter was 2.4 per cent (measured value) a figure of 1.2 per cent was used in estimating the power loss between the vanes and the output flange. All corrections have been applied to the readings of the two wattmeters in such a way that the corrected power measured by each is referred to the output flange of the double-vane wattmeter.

The accuracy claimed for the continuous flow water calorimeter was ± 1.5 per cent and that for the double-vane torque-operated wattmeter was ± 2 per cent at 3.26 cm.

CONCLUSION

The work described in this paper shows that the initial aim of designing a wide-band torque-operated microwave wattmeter has been achieved. The accuracy claimed has been verified by comparison with the best water calorimeter wattmeter available.

The instrument is an absolute standard of power in the microwave band.

ACKNOWLEDGMENT

The authors wish to express their gratitude to Prof. H. M. Barlow for placing at their disposal laboratory facilities of the Electrical Engineering Department of University College, London, in the early stages of development, and for his interest and encouragement in the work. They thank members of the staff of the Wayne-Kerr Laboratories for help in the design of the instrument. Also, they are grateful to the Director of the Radio Research Station of the Department of Scientific and Industrial Research for providing facilities for comparison of the double-vane wattmeter with a water calorimeter wattmeter and to J. Lane for his invaluable assistance in this part of the work. Finally, author S. Okamura is indebted to the British Council for a scholarship which made his part in the work possible.

Traveling-Wave Resonators*

L. J. MILOSEVIC† AND R. VAUTEY†

Summary—**In the first part of the paper, the principles are given which have led to the conception of the traveling-wave resonator, and the calculations enabling its operation to be understood are presented.**

The second part describes the apparatus in detail and examines it, bearing in mind its use as high-power testing equipment.

* Manuscript received by the PGMTT, March 26, 1957; revised manuscript received, December 2, 1957.

† Groupe Éléctronique, Compagnie Française Thomson-Houston, Paris 8, France.

PART I—PRINCIPLE OF OPERATION

INTRODUCTION

THE testing of the power-handling capacity of a microwave transmitter and associated circuit, at far more severe conditions than the nominal ones, has always been considered a very difficult problem for which no valuable solution had been found until the present time.

Two solutions have been proposed to overcome this problem: 1) testing of waveguides at low pressure and 2) testing of waveguides in standing wave. In this case, special hybrid circuits[1] are used for decoupling the magnetron from the circuit to be tested. By means of "cascaded" hybrids the value of apparent power in waveguide is multiplied by 2^n where n is the number of cascaded hybrids.

In the first method, using low pressure conditions, there is no exact relationship between testing and operating conditions. This is due to the fact that the value of breakdown voltage depends upon the nature, pressure, and ionization of the gas, as well as upon the pulse length and repetition rate.

In the second method, using hybrids, the circuit to be tested is placed within the voltage loop of the standing wave. When testing a component, the terminal shorting plunger is moved along $\lambda_g/2$ (where λ_g is the wavelength inside the waveguide) to make sure that every part of the component has actually been subjected to the maximum voltage. In fact, this method suffers from two obvious drawbacks:

1) It is necessary to check voltage handling capacity for each part of the component by moving the shorting plunger, which will increase considerably the duration of test. Furthermore, in the case of intricate components there is still considerable doubt as to the exact value of breakdown voltage.
2) The hybrid circuit increases the test voltage by a $\sqrt{2}$ ratio only. For higher test voltages, the number of hybrids should be increased. This is rather difficult because of the larger number of adjustments required.

Principles of Operation in the Proposed Method

Circuit Using a Hybrid Circuit

A microwave feedback circuit using a hybrid circuit, shown in Fig. 1, has been proposed for use on an electron accelerator.[2]

In this circuit, the transmitter feeds into leg 3 of the hybrid. Incident energy is divided between legs 1 and 2. Leg 1 is connected to a matched load. Leg 2 loops up through waveguide A on to leg 4. The power transmitted along leg 2 is reinjected, therefore, into the hybrid circuit through leg 4. This power is divided between legs 1 and 2 and the process is repeated indefinitely. Leg 3 (transmitter) is decoupled from leg 4 (reinjection) so that the standing-wave ratio, looking from the transmitter, depends upon the hybrid circuit matching conditions and the load on leg 1.

The proper adjustment of the phases, so that the reinjected power will add to the incident power, will result in the storing up of a certain amount of energy within the ring A. Assuming zero attenuation in the ring, the relative voltage level is

$$\frac{1}{(\sqrt{2}-1)} \simeq 2.42.$$

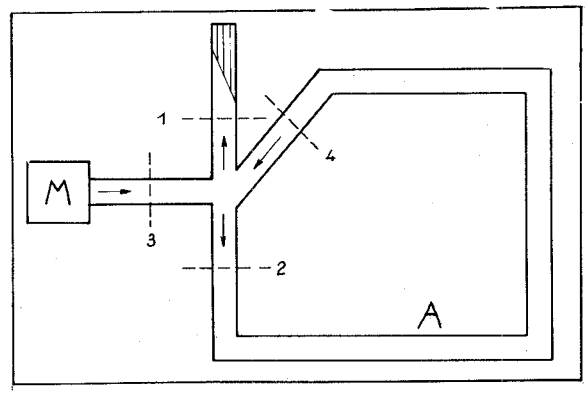

Fig. 1—Microwave feedback circuit.

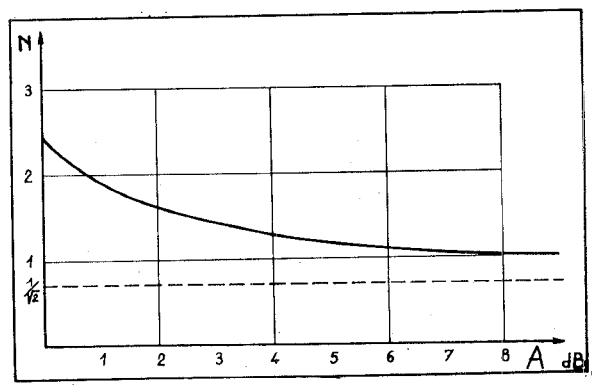

Fig. 2—Overvoltage in the traveling-wave resonator using a hybrid circuit (or a 3-db directional coupler) vs ring attenuation.

For example, with an incident power of 1 mw, the apparent power within the resonator will be

$$1 \text{ mw} \times (2.42)^2 = 5.85 \text{ mw}.$$

When assuming losses equal to A db, the over-voltage coefficient N is given as

$$N = \frac{1}{\sqrt{2} - e^{-\alpha}} \quad \text{with} \quad e^{\alpha} = 10^{A/20}.$$

The curve showing variation of N vs attenuation is shown in Fig. 2.

For easily obtained attenuation values, the overvoltage is slightly greater than 2, but this value, in many cases, is not sufficiently large.

It has proven possible to get higher overvoltage values by modifying the preceding circuit. This has

[1] L. Young, "A hybrid-ring method of simulating higher powers than are available in waveguides," Proc. IEE, vol. 101, pt. III, pp. 189–190; May, 1954.

[2] C. W. Miller, "The design of linear accelerators for X-ray therapy," *Metropolitan Vickers Gazette*, pp. 121–125; December, 1953.

been performed by replacing the hybrid circuit with a directional coupler. The coupling coefficient is adjusted according to the ring attenuation. Thus, the system incorporating a hybrid circuit is now a special case in this more general system.

Circuit of Traveling-Wave Resonator Using a Directional Coupler

Two types of circuits might be proposed, as shown in Fig. 3 and Fig. 4. Maximum N values are identical for both circuits, but the values of optimum coupling coefficient differ in each case.

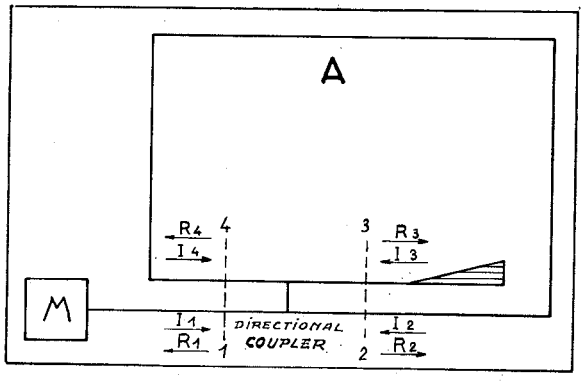

Fig. 3—Microwave feedback circuit with directional coupler—circuit I.

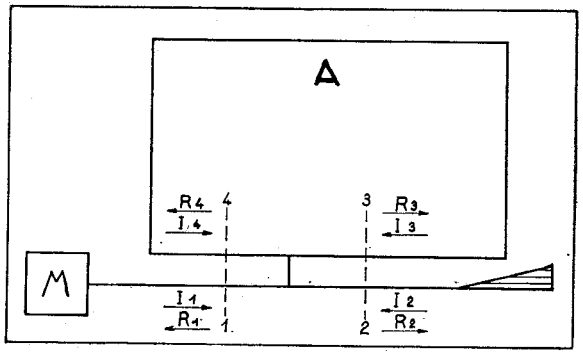

Fig. 4—Microwave feedback circuit with directional coupler—circuit II.

The two circuits in Fig. 3 and Fig. 4 are not grossly different. They could be compared to a conventional resonator connected to a transmission line where the terminals are planes 1 and 3 in Fig. 3, or planes 1 and 2 in Fig. 4.

It is easy to deduce the properties of Fig. 3 from Fig. 4 by inverting planes 2 and 3, which means that C is replaced by $C/(C-1)$. The coupling coefficient C of the directional coupler is expressed as the ratio of the incident power to the transmitted power in the adjacent waveguide. In the design Fig. 3, the greater the losses in the ring, the smaller the coupling coefficient must be for optimum performance.

In the case of Fig. 3, relations between incident and reflected waves are as follows

$$I_4 = R_2 e^{-(\alpha+j\beta)} \tag{1}$$

$$I_3 = R_3 \rho_3 \tag{2}$$

$$I_2 = R_4 e^{-(\alpha+j\beta)}, \tag{3}$$

and in the case of Fig. 4 they are

$$I_4 = R_3 e^{-(\alpha+j\beta)} \tag{4}$$

$$I_2 = R_2 \rho_2 \tag{5}$$

$$I_3 = R_4 e^{-(\alpha+j\beta)} \tag{6}$$

where

I_i = incident-wave amplitudes,
R_i = reflected-wave amplitudes,
ρ_i = reflection coefficients,
$e^{\alpha} = 10^{A/20}$ = attenuation in the ring (A in db),
β = phase shift (in radians) through the ring.

Traveling-Wave Resonator Characteristics

Taking into account (1)–(6), together with the feedback and matching conditions, the traveling-wave resonator characteristics are computed from the scattering matrix of a directional coupler. The matrix of a directional coupler is as follows:

$$\|S_i\| = \begin{Vmatrix} 0 & \frac{\sqrt{C-1}}{\sqrt{C}} & j\frac{1}{\sqrt{C}} & 0 \\ \frac{\sqrt{C-1}}{\sqrt{C}} & 0 & 0 & \frac{j}{\sqrt{C}} \\ j\frac{1}{\sqrt{C}} & 0 & 0 & \frac{\sqrt{C-1}}{\sqrt{C}} \\ 0 & j\frac{1}{\sqrt{C}} & \frac{\sqrt{C-1}}{\sqrt{C}} & 0 \end{Vmatrix}. \tag{7}$$

In the case of the circuit in Fig. 3

$$N = \left|\frac{R_2}{I_1}\right| = \frac{\sqrt{C-1}}{\sqrt{C}-e^{-\alpha}} \tag{8}$$

$$C_{\text{opt}} = e^{2\alpha} \tag{9}$$

$$N_{\max} = \frac{1}{\sqrt{1-e^{-2\alpha}}} = \sqrt{\frac{C_{\text{opt}}}{C_{\text{opt}}-1}}. \tag{10}$$

In the case of the circuit in Fig. 4

$$N = \left|\frac{R_3}{I_1}\right| = \frac{1}{\sqrt{C}-\sqrt{C-1}\cdot e^{-\alpha}} \tag{11}$$

$$C_{\text{opt}} = \frac{1}{1-e^{-2\alpha}} \tag{12}$$

$$N_{\max} = \frac{1}{\sqrt{1-e^{-2\alpha}}} = \sqrt{C_{\text{opt}}}. \tag{13}$$

$N_{\max}$ is identical for both circuits for a given amount of ring attenuation. Variations of $N_{\max}$ and C_{opt} are illustrated in Fig. 5, as a function of ring attenuation A. N has been plotted (dotted curve) for the particular

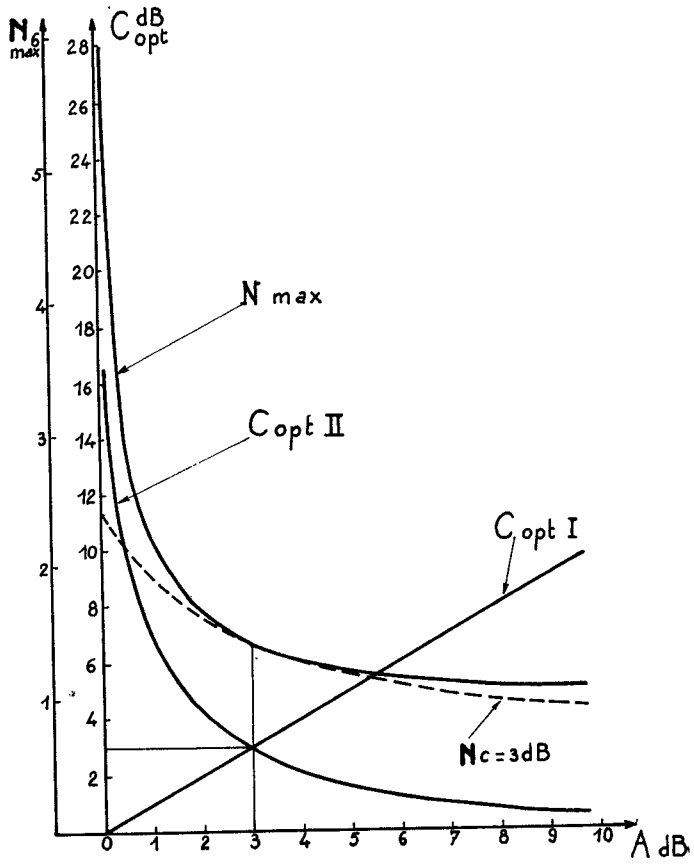

Fig. 5—N_{max}, C_{opt}, and C_{opt} II vs ring attenuation.

case where $C=3$ db. It is to be noticed that this curve meets the N_{max} curve at $A=3$ db.

The microwave resonator is generally of interest when testing low attenuation circuits—say less than 3 db (and even less than 1 db), which is often the case.

In the experimental setup with a variable directional coupler (consisting of, for instance, two 3-db directional couplers and a phase shifter placed in one of the two legs connecting the two 3-db couplers) either circuit may be used depending upon the component to be tested. But, when it is a laboratory model, the first circuit will be preferred because the coupling coefficient is lower and the corresponding directional coupler is easier to make.

The scattering matrix is also useful in studying the reflection coefficient of the ring as seen from the magnetron side.

The reflection coefficient $\rho_1=(R_1/I_1)$ in relation to reflection coefficient ρ_2 (circuit II) is given as:

$$\rho_1=\left|\frac{R_1}{I_1}\right|=\left[\frac{\sqrt{1-\frac{1}{C}}-e^{-\alpha}}{1-\sqrt{1-\frac{1}{C}}\cdot e^{-\alpha i}}\right]^2\rho_2. \tag{14}$$

This value is always less than ρ_2 and equals zero at optimum coupling, thus demonstrating that at optimum coupling the whole incident power is transmitted into the feedback ring and no power is sent into the output load. The insertion loss introduced by the feedback ring, in the case of the permanent circuit, is expressed as

$$\left|\frac{I_1}{R_2}\right|=\frac{1-\sqrt{1-\frac{1}{C}}\cdot e^{-\alpha}}{\sqrt{1-\frac{1}{C}}-e^{-\alpha}}. \tag{15}$$

For optimum coupling conditions, it can be seen that the insertion loss is infinite.

The reflection coefficient in the feedback ring caused by the output load is expressed as

$$\left|\frac{I_3}{R_3}\right|=e^{-\alpha}\frac{\sqrt{1-\frac{1}{C}}-e^{-\alpha}}{1-\sqrt{1-\frac{1}{C}}e^{-\alpha}}\rho_2$$

$$\left|\frac{I_3}{R_3}\right|\ll\rho_2. \tag{16}$$

This coefficient is always smaller than the reflection coefficient of the load.

In any case, in an experimental setup, output load and waveguide mismatches may be corrected by adding a reactor to the ring. By this means the R_4 wave is cancelled before reaching the component to be tested. A monitoring coupler is placed between the reactance and the component in order to check cancellation.

Part II—Description of Practical Resonator

Traveling-Wave Resonator

The practical design of a traveling-wave resonator for microwave operation is illustrated in Fig. 6. Design of circuits is illustrated by the block diagram in Fig. 7.

In this experimental setup, working since July, 1954, in the Microwave Laboratories of the Compagnie Française Thomson-Houston, TH 5657 and TH 5586 magnetrons have been used with a peak power of approximately 800 kw. Power obtained within the resonator varies from 3 to 8 mw depending upon the component under test.[3]

The resonator consists of the following microwave parts, all designed for handling high-microwave power and withstanding air pressure of several kg/cm².

[3] P. J. Sferrazza, "Traveling-wave resonator," *Tele-Tech.*, p. 84; November, 1955. This paper confirms the CFTH laboratory researches described herein.

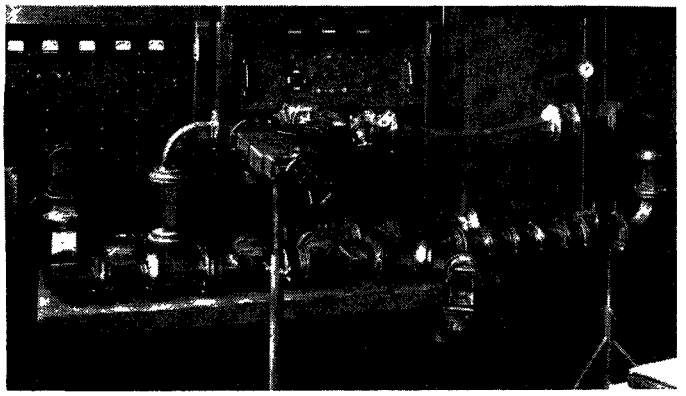

Fig. 6—Photograph of the traveling-wave resonator using a variable directional coupler.

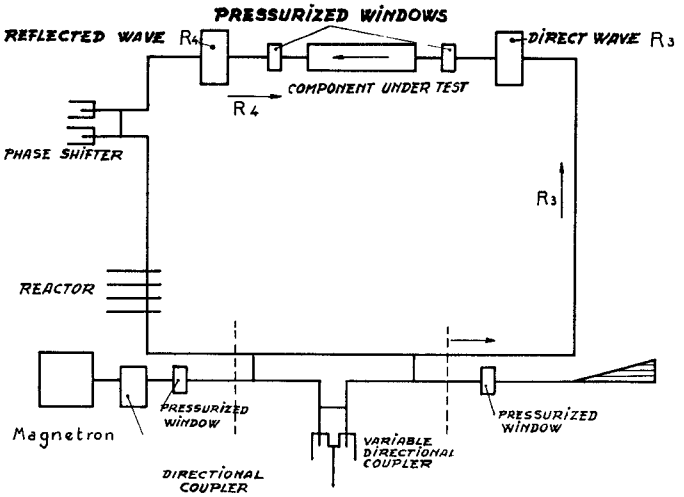

Fig. 7—Schematic diagram of a traveling-wave resonator.

Phase shifter,
Reactor,
Variable directional coupler,
Measuring directional couplers,
Pressurized windows.

Phase Shifter

In traveling-wave resonators, the phase shifter enables the adjustment of the length of the feedback loop to obtain resonance conditions.

The unit consists of a 3-db directional coupler and of two identical plungers simultaneously moved in order to insure a common shorting plane (see Fig. 8).

Assuming that a signal I is sent into leg 1 and that leg 4 is correctly matched, by writing (7) which can be expressed as:

$$\|R\| = \|S_r\| \cdot \|I\|$$

with

$$\|S_r\| = \|S_i^*\|$$

for the 3-db coupler, and allowing for the required connection conditions

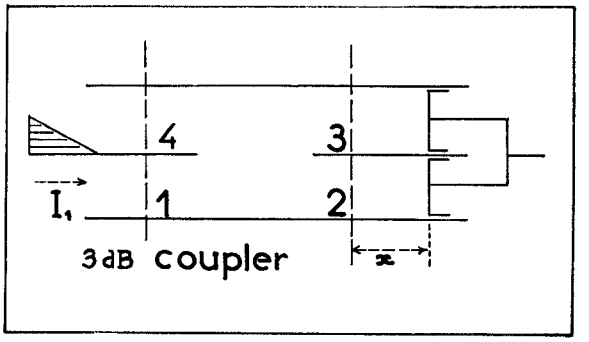

Fig. 8—Circuit diagram of phase shifter.

$$I_2 = R_2 e^{-2j\beta x}$$

$$I_3 = R_3 e^{-2j\beta x}$$

$$I_4 = 0$$

with

$$\beta = \frac{2\pi}{\lambda_g},$$

we obtain

$$\|R\| = \left\| \begin{array}{c} 0 \\ \frac{I_1}{\sqrt{2}} \\ j\frac{I_1}{\sqrt{2}} \\ jI_1 e^{-2j\beta x} \end{array} \right\|.$$

Therefore, the system is correctly matched ($R=0$) and by moving the plungers by Δx, the following phase shift is obtained

$$\Delta\phi = 2\beta\Delta x.$$

The experimented resonator operates over a 2700 to 3100-mc band: maximum plunger elongation is 100 mm and total phase shift is 400°. Power-handling capacity is good, the only limitation being given by the power handling of the 3-db coupler: approximately 3 mw at atmospheric pressure. With a pressure[4] of 2 kg/cm² 8 mw were recorded, without any sign of breakdown discharge.

Reactor

The reactor is used for cancelling wave R_4 (see Fig. 7) before reaching the output plane of component under test. Two types of reactor may be used.

Plunger Reactor: By displacing both plungers of the preceding design in either direction respectively we may use this design as a reactor (see Fig. 9).

[4] All pressure figures are gauge pressure readings.

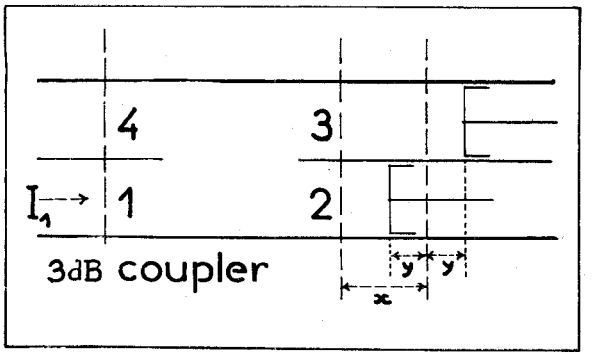

Fig. 9—Circuit diagram of plunger reactor.

In such a case, correct connection conditions are now

$$I_2 = R_2 e^{-2j\beta(x-y)}$$
$$I_3 = R_3 e^{-2j\beta(x+y)}$$
$$I_4 = 0.$$

The same computation, starting from

$$\|R\| = \|S_r\| \cdot \|I\|$$

as before gives

$$\|R\| = \begin{Vmatrix} -jI_1 e^{-2j\beta x} \sin 2\beta y \\ \dfrac{I_1}{\sqrt{2}} \\ j\dfrac{I_1}{\sqrt{2}} \\ jI_1 e^{j\beta x} \cos 2\beta y \end{Vmatrix}.$$

The reflection coefficient in leg 1 is therefore:

$$\rho = \frac{R_1}{I_1} = -je^{-2j\beta x} \sin 2\beta y.$$

Plunger offsetting adjustment ($2y$) makes it possible to vary the standing-wave ratio in leg 1.

$$|\rho| = 0 \text{ if } y = 0 \quad \text{and} \quad |\rho| = 1 \text{ if } y = \frac{\lambda_g}{8}$$

whereas x adjustments alter the phase of the reflected wave.

This circuit shows the advantage of two independent adjustments, namely, as a phase-shifter and reactor.

In the operating reactor shown in Fig. 10, the displacement y can vary over a 0–45 mm range, that is, slightly more than $\lambda_g/8$. Power trials were carried out with a 5-mw magnetron, with a standing-wave ratio of 1.5 and a pressure of 2 kg/cm^2.

Quartz Rod Reactor: This reactor consists of four cylindrical rods made of fused silica; the diameter of the rods is 12 mm and the length is 80 mm. These silica rods are parallel to the wide side of the waveguide and perpendicular to the propagation direction. Distance between the rods is 17.5 mm which is equal to $\lambda_g/8$ at 3000 mc. Total displacement is slightly greater than half the width of waveguide. This design insures proper matching of any standing-wave ratio (vswr) up to 2. The power-handling capacity is superior to the conventional reactor (where the dielectric rods are perpendicular to the wide side of waveguide).

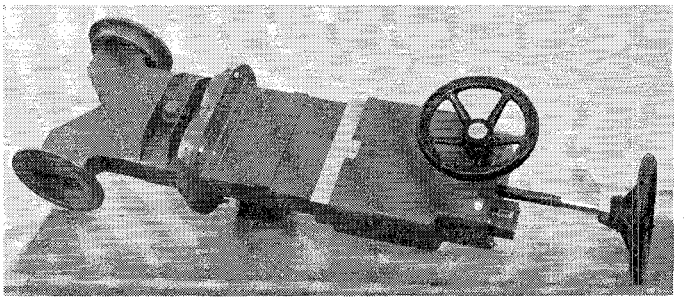

Fig. 10—Photograph of plunger reactor.

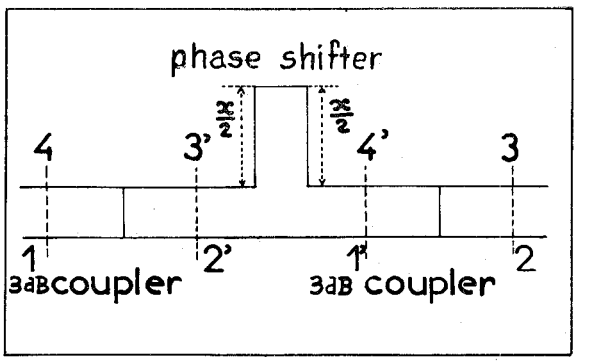

Fig. 11—Circuit diagram of variable directional coupler.

Tests have been conducted successfully with a peak power of 2.5 mw (at normal pressure and a vswr equal to 2 before matching).

In the same conditions, the conventional reactor did not operate above 1.7 mw.

Variable Directional Coupler

This directional coupler makes it possible to adjust the coupling between the main guide and the feedback loop, for the optimum value C_{opt}.

The system consists of two 3-db couplers mounted in cascade and a phase shifter inserted in one of the connecting legs of the 3-db couplers.

A study of the diagram in Fig. 11 shows that the system has the same directional properties as an individual 3-db coupler. Now, assuming x, the path difference between legs (2′–1′) and (3′–4′), coupling conditions are expressed by:

$$I_{1'} = R_{2'} \qquad I_{3'} = e^{-j\beta x} \cdot R_{4'}$$
$$I_{2'} = R_{1'} \qquad I_{4'} = e^{-j\beta x} \cdot R_{3'}.$$

By taking into account the preceding conditions and writing for each 3-db coupler the (7) relation, the following equation is obtained:

$$\begin{vmatrix} I_1 \\ I_2 \\ I_3 \\ I_4 \end{vmatrix} = (S') \begin{vmatrix} R_1 \\ R_2 \\ R_3 \\ R_4 \end{vmatrix}$$

with:

$$(S') = \begin{vmatrix} 0 & e^{j(\pi/2-\beta x/2)} \sin\frac{\beta x}{2} & je^{-j(\beta x/2)} \cos\frac{\beta x}{2} & 0 \\ e^{j(\pi/2-\beta x/2)} \sin\frac{\beta x}{2} & 0 & 0 & je^{-j(\beta x/2)} \cos\frac{\beta x}{2} \\ je^{-j(\beta x/2)} \cos\frac{\beta x}{2} & 0 & 0 & e^{-j(\pi/2+\beta x/2)} \sin\frac{\beta x}{2} \\ 0 & je^{-j(\beta x/2)} \cos\frac{\beta x}{2} & e^{-j(\pi/2+\beta x/2)} \sin\frac{\beta x}{2} & 0 \end{vmatrix}.$$

With a reference plane shift, as given in the diagonal matrix

$$(P) = \begin{matrix} a & 0 & 0 & 0 \\ 0 & b & 0 & 0 \\ 0 & 0 & c & 0 \\ 0 & 0 & 0 & d \end{matrix}$$

it is possible to write this new scattering matrix:

$$(S'') = (P)(S')(P).$$

Putting

$$a = 1 \qquad b = e^{j(\beta x/2-\pi/2)}$$

$$c = e^{j(\beta x/2)}$$

and

$$d = e^{j(\pi/2)}$$

the matrix (S'') may be written

$$\|S''\| = \left\| \begin{matrix} 0 & \sin\frac{\beta x}{2} & j\cos\frac{\beta x}{2} & 0 \\ \sin\frac{\beta x}{2} & 0 & 0 & j\cos\frac{\beta x}{2} \\ j\cos\frac{\beta x}{2} & 0 & 0 & \sin\frac{\beta x}{2} \\ 0 & j\cos\frac{\beta x}{2} & \sin\frac{\beta x}{2} & 0 \end{matrix} \right\|,$$

which proves that the described circuit is working in the same way as a directional coupler having a coupling value of

$$C = \frac{1}{\cos^2\frac{\beta x}{2}}.$$

By simply making x vary between 0 and $\lambda_g/2$ the complete range of coupling values may be covered.

Pressurized Window

Two materials have been tested. The first one was fused silica; the second one was teflon in the form of a sheet several millimeters thick.

A dielectric window into a waveguide is equivalent to a shunting capacitor. In order to match this over a wide band, the height of guide was increased on each side of the dielectric sheet and the length was adjusted in order to obtain the proper series inductance L_1. Shunting inductances L_2 consisting of rods, are also inserted at the point of height discontinuity. The corresponding diagram is shown in Fig. 12. All sharp edges due to waveguide section variations have been carefully rounded.

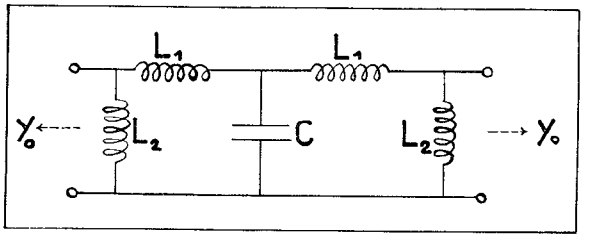

Fig. 12—Matching the pressurized window.

A standing-wave ratio of 1.02 is obtained between 2700 and 3300 mc. Two quartz windows were used during power tests to permit pressurization in the resonator. The test space between the two windows was at atmospheric pressure. Breakdown discharge occurred at a power between 5 and 6 mw.

The teflon window was tested at atmospheric pressure. During test, the window was placed between two quartz windows. The remaining section of the resonator was under higher pressure. At 6 mw, breakdown discharge occurred in the waveguide as well as in the teflon

and quartz windows. The quartz window can withstand relative pressures up to 2 kg/cm² (we experienced quartz failure once at 3.5 kg/cm² and once at 4 kg/cm²). The teflon window has already withstood a relative pressure of 4.5 kg/cm², but further tests are still in progress.

Conclusion

The principles of operation of a traveling-wave resonator designed by the authors have been described. Constituent elements have been discussed and the application to high-power tests was mentioned. Now the fact is stressed that power-handling testing is not the sole application of traveling-wave resonators. This circuit may also be used for other types of measurements. For instance, in the case of optimum coupling, attenuation introduced in the main waveguide is infinite and variation of attenuation within main waveguide aorund this value is very rapid. This can be applied to measurement of low variations in attenuation when studying surface treatments for waveguide, gas tube losses, etc.

Bibliography

[1] Cohn, S. B. and Coale, F. S. "Directional Channel-Separation Filters," Proceedings of the IRE, Vol. 44 (August, 1956), pp. 1018–1024.
[2] Coale, F. S. "A Travelling-Wave Directional Filter," IRE Transactions on Microwave Theory and Techniques, Vol. 4 (October, 1956), pp. 256–260.
[3] Tischer, F. J. "Resonance Properties of Ring Circuits," IRE Transactions on Microwave Theory and Techniques, Vol. 5 (January, 1957), pp. 51–56.

Reflection Coefficient of *E*-Plane Tapered Waveguides*

KATSU MATSUMARU†

Summary—**This paper treats the reflection of linearly and sinusoidally tapered waveguides. In the first part, reflection coefficients of linearly tapered waveguides for dominant modes are calculated. Graphs of the vswr of tapers for different impedance ratios are plotted showing that the vswr does not go to unity at multiples of a half wavelength. In the second part, reflection coefficients of sinusoidally tapered waveguides are calculated. Experimental data verify the theory for both kinds of tapers of various lengths at 4 kmc band.**

Linear tapers perform almost as well as exponential tapers, and better than shorter hyperbolic tapers. The reflection coefficients of sinusoidal tapers can be about half as small as that of the linear tapers, and these tapers compare favorably with the Dolph-Tchebycheff and the Willis taper of improved design.

Introduction

REFLECTION coefficients of tapered waveguides can be calculated by formulas described in the references,[1,2] but these formulas give only rough values. Reflections of several nonuniform transmission lines were theoretically treated by Burrow,[3] Scott,[4] Klopfenstein,[5] Collin,[6,7] Willis and Sinha,[8] Bolinder,[9,10] and others. Most papers treat the magnitudes of reflection coefficient of particular tapers that are mathematically convenient to analyze, but in microwave circuit we often need practical formulas and convenient graphs to determine the reflection coefficients. These several papers are mainly theoretical, with very limited experimental data on tapered waveguides.

In the first part of this paper, approximate theoretical calculations of the reflection coefficient of linear tapers are presented. From the derived formulas, useful graphs were compiled in terms of the suitable ratios of input-to-output surge impedances. To confirm the formulas experimentally at 4 kmc, we have made two groups of tapers in which the ratios of surge impedances are 2.0 and 2.4. The agreement between calculated and

* Manuscript received by the PGMTT, April 12, 1957; revised manuscript received, October 29, 1957.
† Elec. Commun. Lab., Nippon Telegraph and Telephone Public Corp., Tokyo, Japan.
[1] T. Moreno, "Microwave Transmission Design Data," McGraw-Hill Book Co., Inc., New York, N. Y., p. 53; 1948.
[2] G. L. Ragan, "Microwave Transmission Circuit," McGraw-Hill Book Co., Inc., New York, N. Y., M.I.T. Rad. Lab. Ser., vol. 9, p. 305; 1948.
[3] C. R. Burrow, "The exponential transmission line," *Bell Sys. Tech. J.*, vol. 17, pp. 555–573; October, 1938.
[4] H. J. Scott, "The hyperbolic transmission line as a matching section," Proc. IRE, vol. 41, pp. 1654–1657; November, 1953.
[5] R. W. Klopfenstein, "A transmission line taper of improved design," Proc. IRE, vol. 44, pp. 31–35; January, 1956.
[6] R. E. Collin, "The theory and design of wide-band multisection quarter-wave transformer," Proc. IRE, vol. 43, pp. 179–185; February, 1955.
[7] R. E. Collin, "The optimum tapered transmission line matching section," Proc. IRE, vol. 44, pp. 539–548; April, 1956.
[8] J. Willis and N. K. Sinha, "Non-uniform transmission lines as impedance transformers," *Proc. IEE*, pt. B, vol. 103, pp. 166–172; March, 1956.
[9] F. Bolinder, "Fourier transformers in the theory of inhomogeneous transmission lines," Proc. IRE, vol. 38, p. 1354; November, 1950.
[10] F. Bolinder, "Fourier transforms in the theory of inhomogeneous transmission lines," *Trans. Roy. Inst. Tech., Stockholm*, No. 48; 1951.